Clinical Science (2023) **137** 1431–1449
https://doi.org/10.1042/CS20230544

PORTLAND PRESS

Research Article

Transferrin promotes chondrogenic differentiation in condylar growth through inducing autophagy via ULK1-ATG16L1 axis

Xi Wen[1], Yixiang Wang[2] and Yan Gu[1]

[1]Department of Orthodontics, Peking University School and Hospital of Stomatology and National Center of Stomatology and National Clinical Research Center for Oral Diseases and National Engineering Laboratory for Digital and Material Technology of Stomatology, Beijing, China; [2]Central Laboratory, Peking University School and Hospital of Stomatology and National Center of Stomatology and National Clinical Research Center for Oral Diseases and National Engineering Laboratory for Digital and Material Technology of Stomatology, Beijing, China

Correspondence: Yixiang Wang (kqwangyx@bjmu.edu.cn) or Yan Gu (guyan@bjmu.edu.cn)

Skeletal mandibular hypoplasia (SMH) is one of the most common skeletal craniofacial deformities in orthodontics, which was often accompanied by impaired chondrogenesis and increasing apoptosis of condylar chondrocytes. Therefore, protecting chondrocytes from apoptosis and promoting chondrogenesis in condylar growth is vital for treatment of SMH patients. Transferrin (TF) was highly expressed in condylar cartilage of newborn mice and was gradually declined as the condyle ceased growing. Interestingly, serum level of TF in SMH patients was significantly lower than normal subjects. Hence, the aim of our study was to investigate the effect of TF on survival and differentiation of chondrocytes and condylar growth. First, we found that TF protected chondrogenic cell line ATDC5 cells from hypoxia-induced apoptosis and promoted proliferation and chondrogenic differentiation *in vitro*. Second, TF promoted chondrogenic differentiation and survival through activating autophagic flux. Inhibiting autophagic flux markedly blocked the effects of TF. Third, TF significantly activated ULK1-ATG16L1 axis. Silencing either transferrin receptor (TFRC), ULK1/2 or ATG16 significantly blocked the autophagic flux induced by TF, as well as its effect on anti-apoptosis and chondrogenic differentiation. Furthermore, we established an organoid culture model of mandible *ex vivo* and found that TF significantly promoted condylar growth. Taken together, our study unraveled a novel function of TF in condylar growth that TF protected chondrocytes from hypoxia-induced apoptosis and promoted chondrogenic differentiation through inducing autophagy via ULK1-ATG16L1 axis, which demonstrated that TF could be a novel growth factor of condylar growth and shed new light on developing treatment strategy of SMH patients.

Introduction

Skeletal mandibular hypoplasia (SMH) is one of the most common skeletal craniofacial deformities in orthodontics featured by mandible deficiency, unfavorable facial profile and narrow upper airway [1]. Patients with severe SMH could suffer obstructive sleep apnea syndrome (OSAS) leading to compromise life quality [2]. Functional appliances such as Activator and Twin-block appliance are often used to promote mandibular growth. However, controversies still exist in the treatment outcome and stability of functional treatment on SMH [3,4]. Therefore, detecting the pathogenesis of SMH and developing efficient therapy strategies to promote mandibular growth are vital for improving the treatment outcome of SMH patients.

Endochondral ossification of condylar cartilage contributes greatly to the growth and bone mass increment of mandible during postnatal development [5–7]. Chondrocytes in condylar cartilage underwent

Received: 22 May 2023
Revised: 08 September 2023
Accepted: 08 September 2023

Accepted Manuscript online: 11 September 2023
Version of Record published: 21 September 2023

© 2023 The Author(s). Published by Portland Press Limited on behalf of the Biochemical Society

Clinical Science (2023) **137** 1431–1449
https://doi.org/10.1042/CS20230544

proliferation, differentiation and hypertrophic maturation under control of a signaling network, then recruited osteoblast and osteoclast to form the bone trabecula and promoting the increment of mandibular bone mass [8]. Mandibular deficiency was often accompanied by impaired chondrogenesis and increasing apoptosis of condylar chondrocytes [9,10]. Hence, promoting the chondrogenesis and reducing apoptosis of condylar chondrocytes were considered as key therapeutic targets to promote mandibular growth of SMH patients.

Chondrocytes survive in a hypoxic and nutrition deficiency microenvironment [11–13]. Autophagy is an intracellular degradation process induced by stresses and nutrition deprivation, which enables cells to adapt to microenvironment through providing amino acid, glucose and fatty acid, therefore served as an important self-protective mechanism for survival of chondrocytes [14]. Researches showed that defect in autophagy could aggravate the degradation of cartilage matrix and damage of subchondral bone in osteoarthritis [15,16]. Genetic ablation of autophagy protein ATG7 in chondrocytes could cause severe growth retardation [14,17]. Hence, exploring the mechanism by which chondrocytes regulates autophagy to avoid apoptosis under hypoxia and promote chondrogenic differentiation may shed new light on developing strategy to promote mandibular growth.

Transferrin (TF) is a 76 kDa glycoprotein that is produced mainly in liver and could transport iron ion in circulation between sites of absorption, storage and utilization [18]. Although TF is widely believed to be important for iron acquisition by all mammalian cells, its physiological function for mammal's bone development is poorly understood. Lei et al. reported that deficiency of transferrin receptor (TFRC) in cranial neural crest cells would cause mandibular deficiency, but the underlying mechanism still remained unclear [19]. Our preliminary data showed that TF was enriched in condylar cartilage of newborn mice, and was gradually decreased afterbirth. Interestingly, we also found that serum level of TF in SMH subjects was significantly lower than normal subjects, indicating its potential role in regulation of condylar growth and pathology mechanism of SMH.

Here, we reported a novel function of TF in condylar growth that not only prevented cell apoptosis under hypoxic microenvironment (simulated microenvironment of condylar cartilage) but also promoted chondrogenic differentiation via inducing autophagy flux mediated by ULK1-ATG16L1 axis. Furthermore, we created an *ex vivo* culture model of mandible and proved that TF could promote condylar growth at organoid level. Our study aimed to reveal a novel effect of TF on proliferation and differentiation of chondrocytes, thereby advancing our knowledge of the mechanism underlying the development of condylar cartilage and shedding new light on developing treatment strategy of SMH patients.

Materials and methods

Study population

SMH patients and normal control subjects were recruited from patients who sought for orthodontic treatment in Peking University School and Hospital of Stomatology from February 2019 to July 2019. Informed consents were obtained from both patients and their parents. SMH patients were diagnosed according to the criteria as follows: 1. ANB $> 5^{\circ}$; 2. Overjet > 3 mm; 3. Distal molar relationship; 4. No systemic disease. Normal control subjects were defined according to the criteria as follows: 1. $0 <$ ANB $< 5^{\circ}$; 2. $0 <$ Overjet < 3 mm; 3. Neutral molar relationship; 4. No systemic disease. Lateral cephalograms were taken during their first visit. CVM stage (CS) was determined according to the protocol proposed by Baccetti et al. [20]. CVM stage at 3-4 (CS 3-4) were considered as pubertal growth peak. Two different orthodontists assessed the CVM stage separately and inter-observer agreement was calculated. One of two orthodontists evaluated the CVM stage again one week later to assess intra-observer agreement. Both observers were blinded to patients' information.

Serum samples of SMH patients

About 4 ml of venous blood was drawn from each subject during 8:00–10:00 am on their first visit. After placed for 20 min at room temperature, the vacuum tubes were centrifuged at 3000 rpm for 15 min. Then, the supernatant was carefully removed from the blood clot by pipette and transferred into a new centrifuge tube. The minimum sample size was calculated on the basis of the formula applying to a one-way ANOVA two-tailed test proposed by Chow et al. [21].

Animals and tissues collection

All wild-type C57BL/6 male mice were purchased from Beijing Vital River Laboratory Animal Technology (Beijing, China). All animal experiments were conducted in the animal laboratory of Peking University School of Stomatology. All animal procedures were conducted under the approval of Biomedical Ethics Committee of Peking University (LA2021538) and conducted in accordance with the Guide for the Care and Use of Laboratory Animals. After mice

© 2023 The Author(s). Published by Portland Press Limited on behalf of the Biochemical Society

Clinical Science (2023) **137** 1431–1449
https://doi.org/10.1042/CS20230544

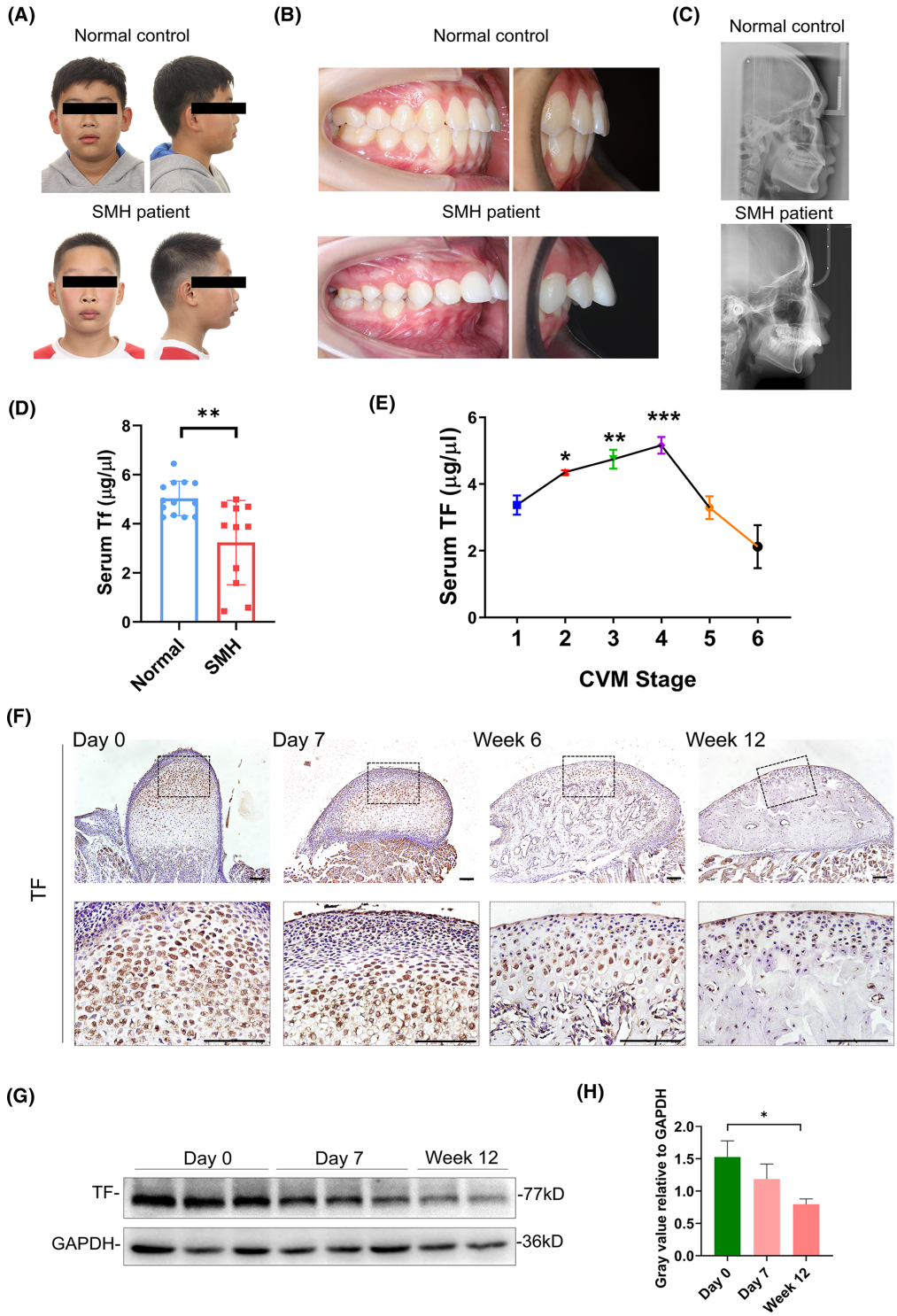

Figure 1. Serum transferrin level of SMH patients at growth peak is significantly lower than normal subjects

(**A**) Facial photographs of SMH patients. (**B**) Intraoral photographs of SMH patients. (**C**) Lateral cephalogram of SMH patients. (**D**) Mean serum TF level of SMH patients at growth peak was significantly lower than that of normal subjects. (**E**) In normal subjects, serum TF level was significantly increased as pubertal growth peak arrived (CS 3-4) and dramatically declined after growth peak ended (CS 5-6). The asterisks indicated the significance of difference compared with CS6. (**F**) Immunohistochemistry staining of TF in condylar cartilage of C57BL/6 mice at postnatal day 0 (Day 0), day 7, week 6 and week 12 (bar = 100 μm). (**G**) Western blot for TF in condylar cartilage of C57BL/6 mice at day 0, day 7 and week 12. (**H**) Quantification of gray value of TF relative to GAPDH. (*: $P<0.05$, **: $P<0.01$, ***: $P<0.001$).

© 2023 The Author(s). Published by Portland Press Limited on behalf of the Biochemical Society

Clinical Science (2023) **137** 1431–1449
https://doi.org/10.1042/CS20230544

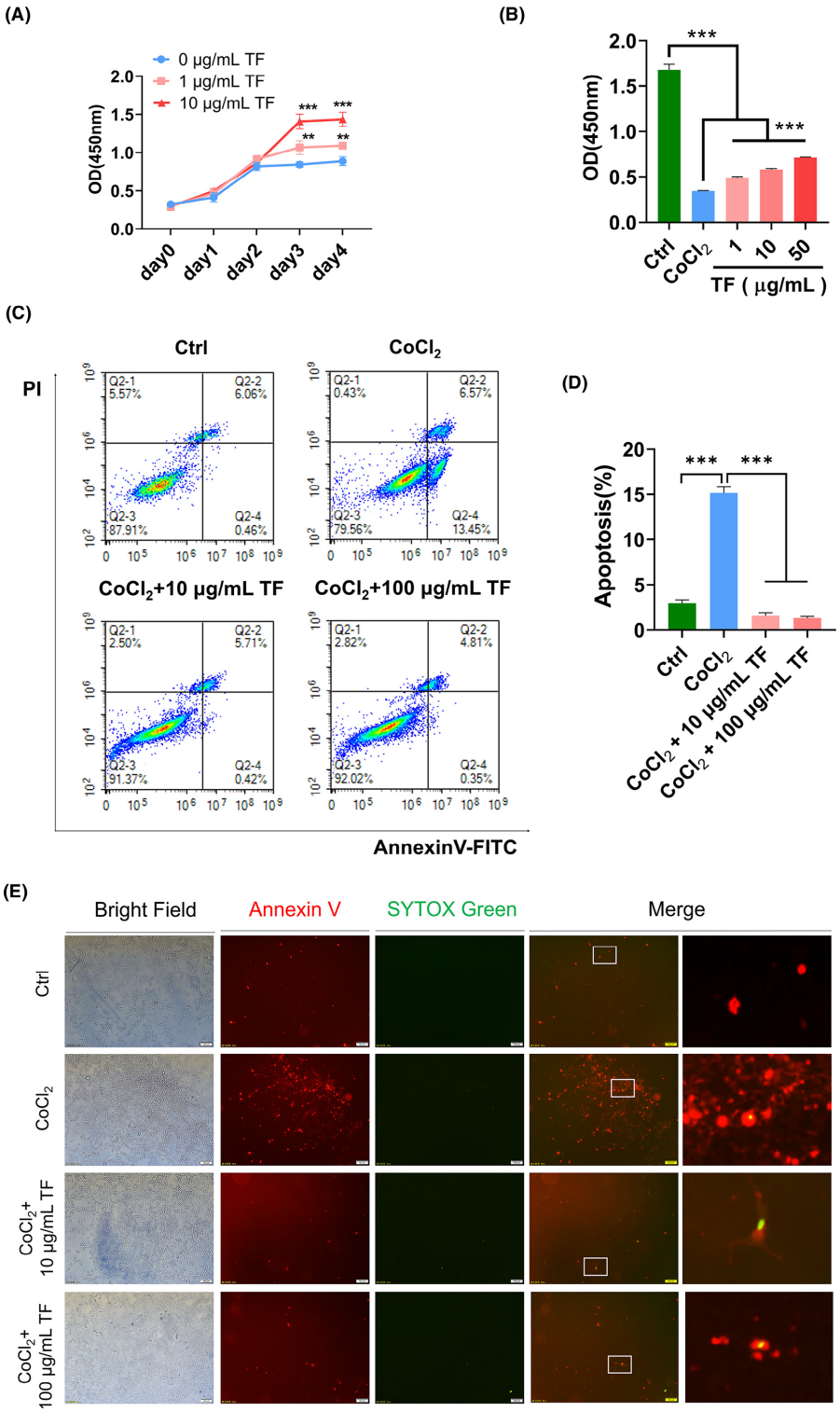

Figure 2. TF not only protects chondrocytes from hypoxia-induced apoptosis, but also promotes chondrocyte proliferation

(**A**) ATDC5 cells were cultured in medium containing 0, 1 and 10 μg/ml TF. CCK8 assay was performed at day 0, day 1, day 2, day 3 and day 4 after cells were seeded. (**B**) $CoCl_2$ was used to treat ATDC5 cells to mimic hypoxia *in vitro*. Cells were cultured in medium containing 0, 1, 10 and 50 μg/ml TF after $CoCl_2$ treatment. CCK8 assay was performed at 24 h after $CoCl_2$ treatment. (**C,D**) Cells were cultured in medium containing 10 and 100 μg/ml TF after $CoCl_2$ treatment. Flow cytometry assay of Annexin V/ PI staining was performed at 24 h after $CoCl_2$ treatment. (**E**) Fluorescence staining of Annexin V-SYTOX was performed at 24 h after $CoCl_2$ treatment (bar = 100 μm) (**: $P<0.01$, ***: $P<0.001$).

© 2023 The Author(s). Published by Portland Press Limited on behalf of the Biochemical Society

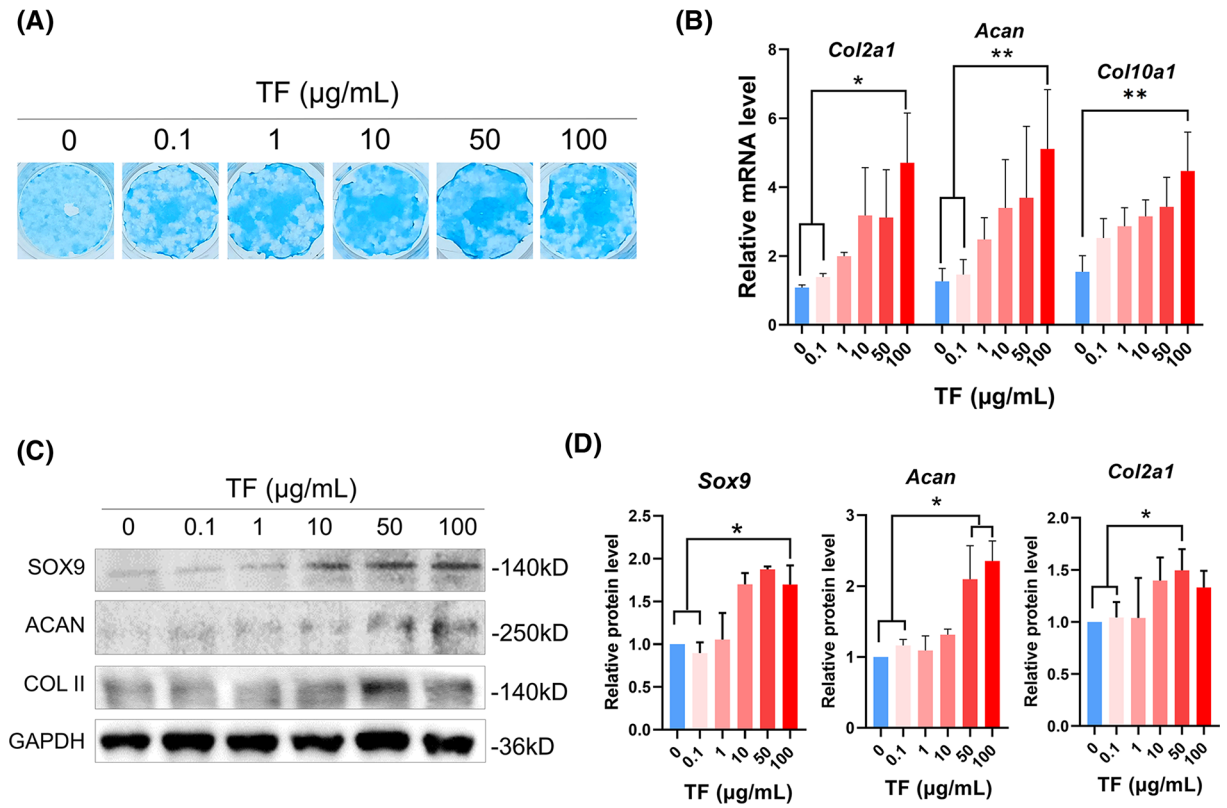

Figure 3. TF promotes chondrogenic differentiation *in vitro*

(**A**) Representative images of alcian staining of ATDC5 cells after cultured in media containing 0, 0.1, 1, 10, 50 and 100 μg/ml TF for 9 days. (**B**) mRNA level of *Col2a1*, *Acan* and *Col10a1* in ATDC5 cells after cultured in media containing 0, 0.1, 1, 10, 50 and 100 μg/ml TF for 9 days. (**C,D**) Protein level of SOX9, ACAN and COL II in ATDC5 cells after cultured in media containing 0, 0.1, 1, 10, 50 and 100 μg/ml TF for 9 days (*: $P<0.05$, **: $P<0.01$).

were killed by cervical dislocation, condyle tissue was fixed by 4% paraformaldehyde for 24 h and decalcified for 1 week, then dehydrated and embedded in paraffin for making tissue slices. For total protein extraction, condyle tissue was dissected and frozen quickly in liquid nitrogen, and then ground into powder in cell lysis buffer. After centrifuged at 12000 ***g*** for 15 min, the supernatant was collected for Western blot assay.

Enzyme-linked immunosorbent assay (ELISA)

ELISA kit of human TF (Qisong Company, Beijing, China) was applied to determine the concentration of TF in serum following the instruction of manufacturer. Each sample required three replicates and the mean value were calculated for further statistical analysis. An El×808 spectrophotometer (BioTek, Hercules, U.S.A.) was used to detect the optical densities (OD_{450}) and calculate the total protein concentration.

Cell culture and transfection

ATDC5 cells were purchased from American Type Culture Collection (ATCC, Manassas, U.S.A.). Cells were cultured in DMEM with 10% fetal bovine serum (growth medium). Growth media containing 0.1, 1, 10, 50 and 100 μg/ml TF (Sigma, T1147, St. Louis, MO, U.S.A.) were prepared respectively to investigate their effects on cell proliferation, apoptosis and chondrogenic differentiation. Cobalt chloride (Sigma, 7646-79-9) was added to mimic hypoxic environment at concentration of 500 μmol/L. 3-MA (Sigma, 5142-23-4) was used to block autophagy flux at concentration of 10 μM. Rapamycin (Sigma, 53123-88-9) was used to activate autophagy flux at concentration of 100 nM. Ad-GFP-LC3B (Beyotime, C3006, Shanghai, China), and Ad-mCherry-GFP-LC3B (Beyotime, C3012) was transfected into cells according to manufacturer's instruction. LysoTracker Green (Beyotime, C1047), LysoTracker Red (Beyotime, C1046) and MitoTracker Red CMXRos (Beyotime, C1049) were loaded into cells at concentration of 100 nM. Small interfering RNAs were designed to knockdown the expression of *Tfr1*, *Ulk1*, *Ulk2* and *Atg16l1*, along with negative control

© 2023 The Author(s). Published by Portland Press Limited on behalf of the Biochemical Society

Clinical Science (2023) **137** 1431–1449
https://doi.org/10.1042/CS20230544

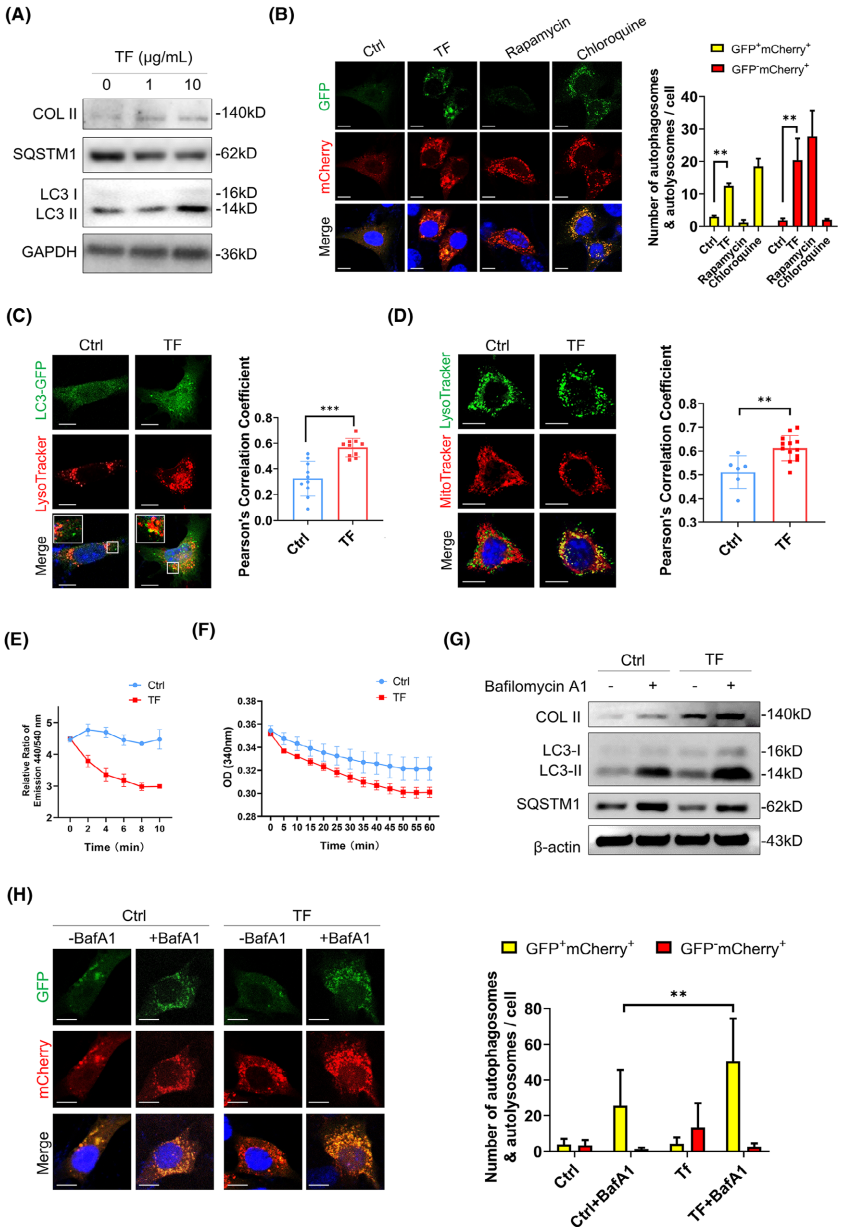

Figure 4. TF stimulates intracellular autophagy flux

(**A**) ATDC5 cells were cultured in medium containing 0, 1 and 10 μg/ml TF. Western blot was performed to analyze the expression of COL II, SQSTM1 and LC3. (**B**) Ad- mCherry-GFP-LC3 was transfected into ATDC5 cells treated with control medium and medium containing 10 μg/ml TF. Rapamycin and chloroquine were used as positive and negative control, respectively. Yellow puncta (GFP+ mCherry+) represented autophagosomes, while red puncta (GFP- mCherry+) represented autolysosomes (bar = 10 μm). (**C**) ATDC5 cells were loaded with LysoTracker Red and LC3-GFP to track the fusion of autophagosome and lysosome (bar = 10 μm). (**D**) ATDC5 cells were loaded with Lyso-Tracker Green and Mito-Tracker Red to detect the lysosomal acidity and engulfment of mitochondria by lysosome. Pearson correlation coefficient was calculated to quantify the co-localization of the fluorescence (bar = 10 μm). (**E**) ATDC5 cells were loaded with LysoSensor DND-160 to detect the lysosomal acidity, which emitted yellow fluorescence at 540 nm in acidic lysosomes and blue fluorescence at 440 nm in less acidic or neutral lysosomes. The ratio of fluorescence intensity at 440 and 540 nm was calculated to detect the lysosomal acidity and V-ATPase activity. (**F**) The activity of V-ATPase of total cell lysates after cultured in control and TF medium was assayed via the decreasing rate of the absorbance of substrates. (**G**) ATDC5 cells were incubated in 100 nM bafilomycin A1 for 4 h after cultured in control and TF medium, and Western blot was performed to analyze the endogenous expression of COL II, SQSTM1 and LC3. (**H**) Ad-mCherry-GFP-LC3 transfected cells were incubated in 100 nM bafilomycin A1 for 4 h after cultured in control and TF medium, and the number of autophagosomes (yellow puncta) and autolysosomes (red puncta) were observed and calculated (**: $P<0.01$, ***: $P<0.001$).

© 2023 The Author(s). Published by Portland Press Limited on behalf of the Biochemical Society

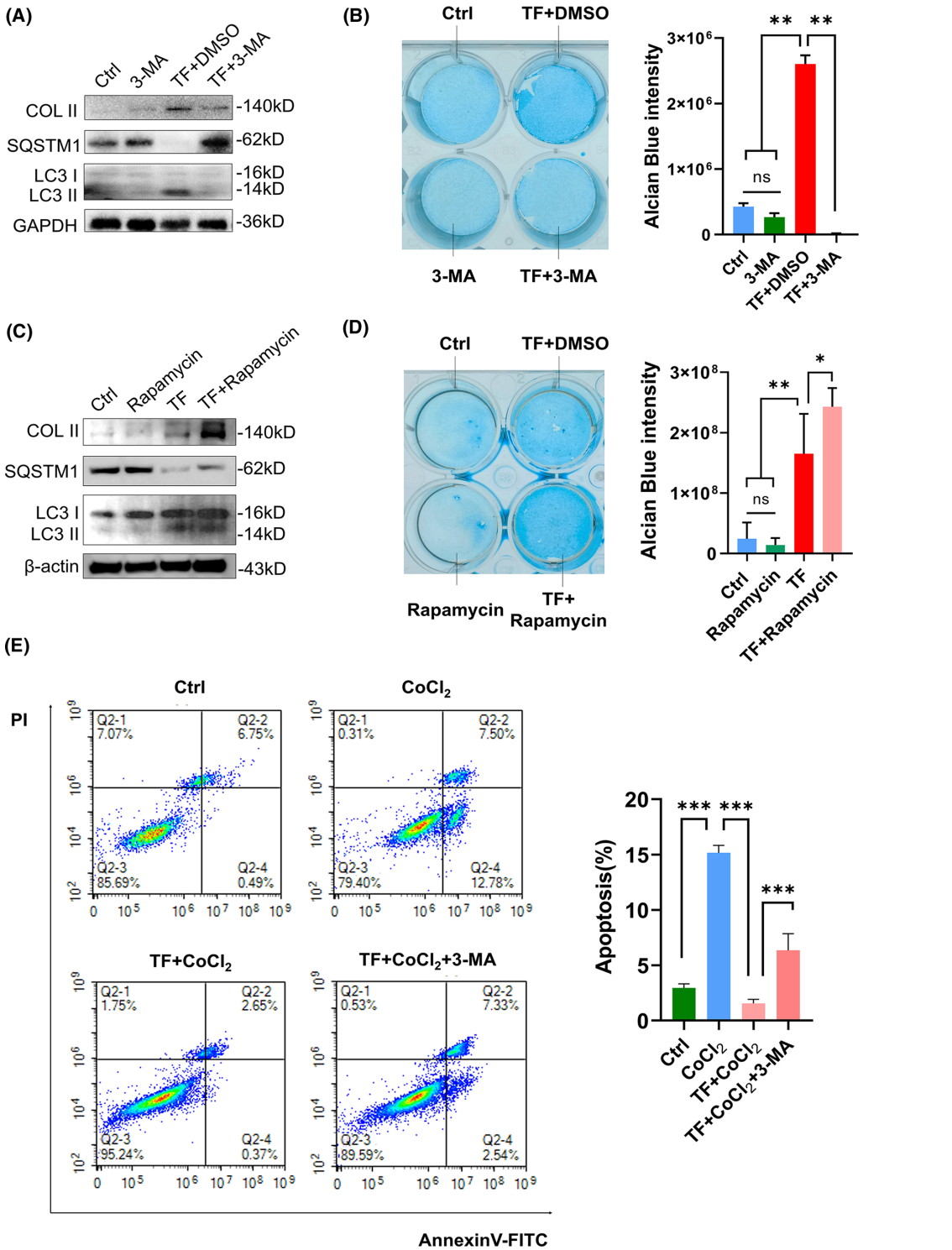

Figure 5. TF induces autophagy flux facilitating chondrogenic differentiation and survival from hypoxia-induced apoptosis

(**A**) 3-MA was added to block the autophagy flux induced by TF and western blot was performed to analyze the expression of COL II, SQSTM1 and LC3. (**B**) Alcian blue staining of ATDC5 cells cultured in control medium, TF medium and TF+3-MA medium for 9 days. The intensity of alcian blue staining was calculated. (**C**) Rapamycin was added to promote autophagy flux induced by TF and western blot was performed to analyze the expression of COL II, SQSTM1 and LC3. (**D**) Alcian blue staining of ATDC5 cells cultured in control medium, TF medium and TF+rapamycin medium for 9 days. The intensity of alcian blue staining was calculated. (**E**) Flow cytometry of annexin V- PI staining of cells treated with control medium, $CoCl_2$, $CoCl_2$+TF and $CoCl_2$+TF+3-MA. The percentage of apoptotic cells was calculated (*: $P<0.05$, **: $P<0.01$, ***: $P<0.001$).

© 2023 The Author(s). Published by Portland Press Limited on behalf of the Biochemical Society

Clinical Science (2023) **137** 1431–1449
https://doi.org/10.1042/CS20230544

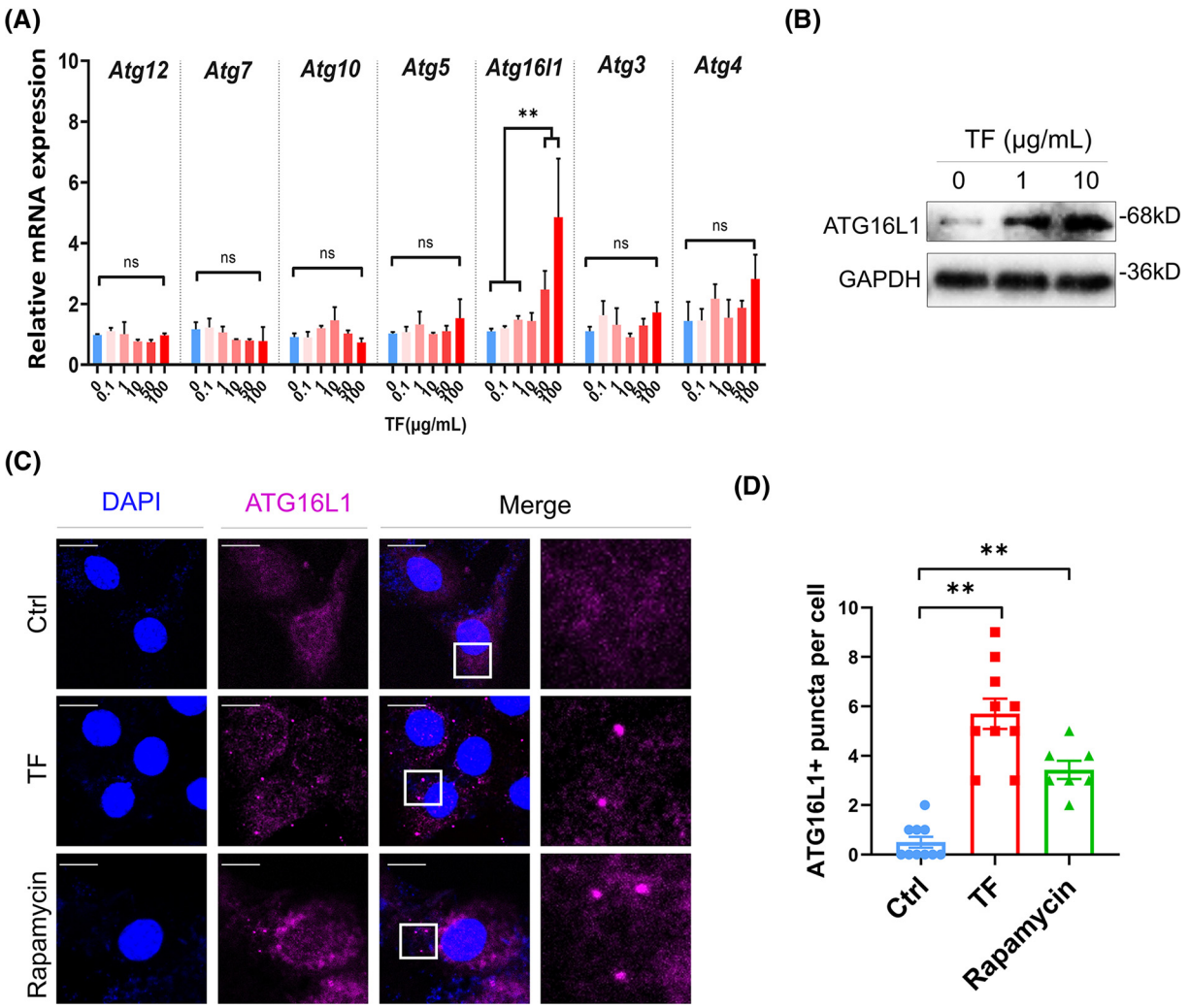

Figure 6. TF induces the expression of ATG16L1

(**A**) The mRNA expression level of main autophagy-related genes (ATGs) in cells cultured in medium containing 0, 0.1, 1, 10, 50 and 100 μg/ml TF were analyzed by real-time PCR. The mRNA expression level of *Atg16l1* was found to increase significantly after cultured in medium containing TF. (**B**) Western blot was performed to examine the protein level of ATG16L1 in cells cultured in media with 0, 1 and 10 μg/ml TF, respectively. (**C**) Immunofluorescence staining of ATG16L1 in cells cultured in control medium and medium containing 10 μg/ml TF. Rapamycin was used as a positive control. (**D**) Quantitative result of immunofluorescence staining of ATG16L1. The number of ATG16L1+ puncta was significantly higher than control group. (**: $P<0.01$).

Table 1 siRNA sequences used for knock-down of *Tfr1*, *Ulk1*, *Ulk2* and *Atg16l1*

Gene	Sense (5′→3′)	Antisense (5′→3′)
Tfr1	GGAUAUGGGUCUAAGUCUATT	UAGACUUAGACCCAUAUCCTT
Ulk1	GCCUCAGCUUGCGACUUCA	UGAAGUCGCAAGCUGAGGC
Ulk2	CACGGUACCUACAUAGUAA	UUACUAUGUAGGUACCGUG
Atg16l1	GACUGUGGAUGAUUAUCGA	UCGAUAAUCAUCCACAGUC

(siNC) with a scramble sequence (Table 1). Transfection reagent jetPRIME (Polyplus-Transfection, Illkirch, France) was used to transfect siRNA into ATDC5 cell line.

© 2023 The Author(s). Published by Portland Press Limited on behalf of the Biochemical Society

Table 2 Primers used for qRT-PCR

Gene	Sense (5′-3′)	Antisense (5′-3′)
Sox9	ATGAATCTCCTGGACCCCTT	CTTCCTCGCTCTCCCTCTTC
Col2a1	TACAGGGAATGCCTGGTGAG	AGGTCCGACTTCTCCCTTCTC
Acan	AGTTCTTGGAGGAGCGAGTC	GTTGTCATGGTCTGGAACTT
Col10a1	TTCTGCTGCTAATGTTCTTGACC	GGGATGAAGTATTGTGTCTTGGG
Atg12	TGACACACTGGAGGATGTGC	ATGAGGCGCAAGAACCAGAA
Atg7	GTTCGCCCCCTTTAATAGTGC	TGAACTCCAACGTCAAGCGG
Atg10	GTAGTTACCAAGTGCCGGTTC	AGCTAACGGTCTCCCATCTAAA
Atg5	TGTGCTTCGAGATGTGTGGTT	GTCAAATAGCTGACTCTTGGCAA
Atg16l1	CAGAGCAGCTACTAAGCGACT	AAAAGGGGAGATTCGGACAGA
Atg3	ACACGGTGAAGGGAAAGGC	TGGTGGACTAAGTGATCTCCAG
Atg4	GCTGGTATGGATTCTGGGGAA	TGGGTTGTTCTTTTTGTCTCTCC
Gapdh	AGGTCGGTGTGAACGGATTTG	GGGGTCGTTGATGGCAACA

Real-time quantitative polymerase chain reaction and Western blot

Total RNA of cell lysate was extracted using Trizol Reagent (Vazyme, Nanjing, China). Approximately 1 μg of RNA was used for reverse transcription and cDNA synthesis (Vazyme, Nanjing, China). qPCR was performed using SYBR green PCR master mix (Vazyme, Nanjing, China). Sequences of primers were listed in Table 2. Total protein of cell lysate was extracted using radioimmunoprecipitation assay (RIPA) lysis buffer comprising of 50 mM Tris-HCl (pH 7.4), 150 mM NaCl, 1% Triton X-100, 1% sodium deoxycholate and 0.1% SDS (Solarbio, R0010, Beijing, China) containing 1% protease inhibitors phenylmethylsulfonyl fluoride (Solarbio, P0100). Total protein of cell lysate was centrifuged at 12,000 rpm for 30 min, and the supernatant was collected for protein quantification using BCA assay kit (Beyotime, P0009). Approximately 30 μg protein was separated by electrophoresis using 10% Tris-Glycine gel (Beyotime, P0052A) under constant voltage of 120 V for 30 min. After electrophoresis, protein was transfer to polyvinylidene difluoride (PVDF) membrane under constant current of 220 mA for 2 h. The membrane was then blocked by 5% BSA for 1 h at room temperature and was incubated with primary antibodies at 4°C overnight. Primary antibodies were as follows: TF (Proteintech, 17435-1-AP, 1:1000, IL, U.S.A.), SOX9 (Proteintech, 67439-1-Ig, 1:1000), COL II (Santa Cruz, M2139, 1:500, Texas, U.S.A.), ACAN (Proteintech, 13880-1-AP, 1:1000), LC3A/B (Cell Signaling Technology, 12741, 1:1000, MA, U.S.A.), SQSTM1 (Abcam, 109012, 1:1000, Cambridge, U.K.), TFRC (Abcam, ab214039, 1:1000), ULK1 (Cell Signaling Technology, 8054, 1:1000), Phospho-ULK1(Ser555) (Cell Signaling Technology, 5869, 1:1000), AMPKα (Cell Signaling Technology, 5831, 1:1000), Phospho-AMPKα (Thr172) (Cell Signaling Technology, 74281, 1:1000), ATG16L1 (Cell Signaling Technology, 8089, 1:1000), and GAPDH (Abcam, 181602, 1:1000, Cambridge). After washed by Tris-buffered saline containing 0.1% Tween-20 detergent (TBST), membrane was incubated with corresponding HRP-conjugated secondary antibody (Solarbio, SE134, 1:10000, Beijing, China) for 1 h before exposure.

Histology and immune staining

Tissues were fixed in 4% paraformaldehyde (PFA) (Solarbio, P1110) and were embedded in paraffin (Leica, P3683, Germany). The melting point of paraffin was at 56–58°C. Serial paraffin-embedded sections of 5 μm thickness were obtained from dorsal-ventral aspects of the condylar cartilage. Before histology and immune staining, paraffin sections (5 μm) were deparaffinized. Antigen recovery were performed using 0.25% trypsin and proteinase K (Solarbio, P1120,1:1000). Toluidine blue staining was performed using assay kit (Solarbio, G3668) according to standard protocols of the manufacturer's instructions. As for immunohistochemistry staining, primary antibodies were as follows: COL II (Santa Cruz, M2139,1:200) and ACAN (Proteintech, 13880-1-AP, 1:200). HRP-conjugated secondary antibody (ZSGB-BIO, PV9001, Beijing, China) and DAB kit (Solarbio, DA1010) were used according to manufacturer's instruction.

Cells were plated on micro cover glasses (Solarbio, YA0350). After treatment, cells were washed with phosphate buffer solution (PBS) (Solarbio, P1020) and fixed with 4% PFA (Solarbio, P1110) for 10 min. The cells were permeabilized by 0.3% Triton X-100 (Solarbio, T8200) for 10 min, and blocked in 5% BSA (Solarbio, A8020), then incubated with primary antibodies (ATG16L1, Cell Signaling Technology, 8089, 1:1000) overnight at 4°C. Slides were washed and incubated with Fluor647 (Affinity, S0013, 1:200, Nanjing, China) at room temperature for 1 h. Photomicrographs were taken using a confocal microscope (Leica TCS-SP8, Germany).

© 2023 The Author(s). Published by Portland Press Limited on behalf of the Biochemical Society

Clinical Science (2023) **137** 1431–1449
https://doi.org/10.1042/CS20230544

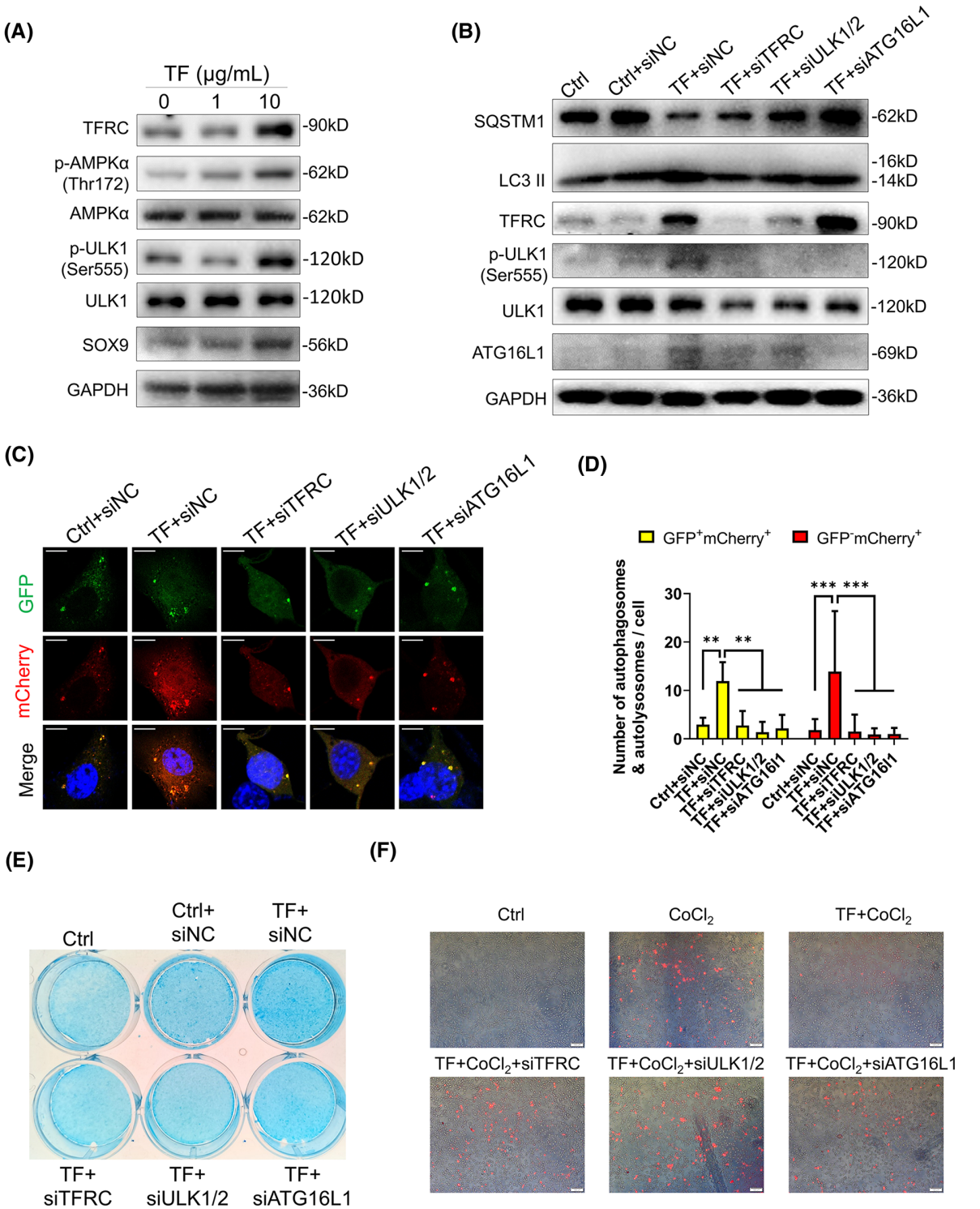

Figure 7. TF stimulates autophagy flux via ULK1-ATG16L1 pathway

(**A**) Western blots for TFRC, phospho-AMPKThr172, phospho-ULK1Ser555 and SOX9 in cells cultured in media with 0, 1 and 10 μg/ml. (**B**) Western blots for SQSTM1, LC3, TFRC, phospho-ULK1Ser555, ULK1 and ATG16L1 in cells transfected with siRNA against *Tfr1*, *Ulk1/2* and *Atg16l1*. (**C**) Ad-LC3-mCherry-GFP was transfected into cells in which *Tfr1*, *Ulk1/2* and *Atg16l1* were silenced, respectively. (**D**) The number of autophagosomes (GFP+, mCherry+) and autolysosomes (GFP-, mCherry+) in each group. (**E**) Alcian blue staining of cells cultured in medium containing 10 μg/ml TF after *Tfr1*, *Ulk1/2* or *Atg16l1* was silenced. (**F**) Fluorescence staining of annexin V/SYTOX in cells cultured in $CoCl_2$+TF medium after *Tfr1*, *Ulk1/2* or *Atg16l1* was knocked down (bar = 100 μm) (**: $P<0.01$, ***: $P<0.001$).

© 2023 The Author(s). Published by Portland Press Limited on behalf of the Biochemical Society

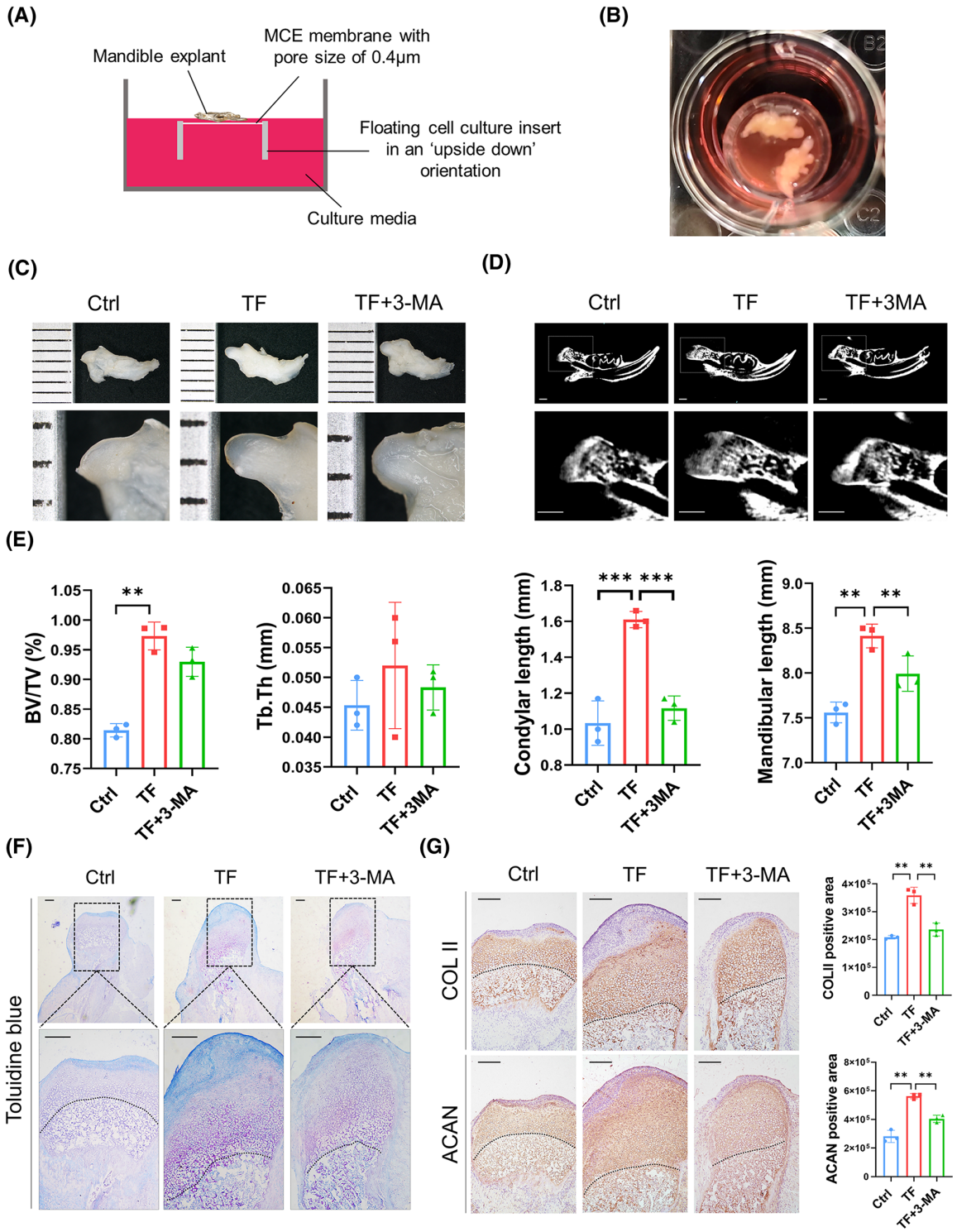

Figure 8. TF promotes condylar growth and chondrogenesis of mandible organoid

(**A**) Illustration of organoid culture of mandible. (**B**) Photograph of organoid culture of mandible. (**C**) The morphology of condylar cartilage after cultured in control medium, TF medium and TF+3MA medium for 7 days. (**D**) Representative images of micro-CT reconstruction of mandible organoid. The white square indicated the condyle area. (**E**) Micro-CT analysis of bone volume/total volume (BV/TV), trabecular thickness (Tb.Th), the length of condyle and the total length of the mandible (**: $P<0.01$; ***: $P<0.001$). (**F**) Toluidine blue staining of condylar cartilage. Dotted line indicated the boundary of condylar cartilage and subchondral bone (bar = 200 μm). (**G**) Immunohistochemistry staining of COL II and ACAN in condylar cartilage. Dotted line indicated the boundary of condylar cartilage and subchondral bone (bar = 200 μm, **: $P<0.01$; ***: $P<0.001$).

© 2023 The Author(s). Published by Portland Press Limited on behalf of the Biochemical Society

Clinical Science (2023) **137** 1431–1449
https://doi.org/10.1042/CS20230544

Table 3 Parameters of recruited SMH patients and normal subjects at pubertal peak

	Control	SMH	*P*-values
Number of cases	14	11	/
Gender (M/F)	8/6	5/6	/
Age	11.43 ± 2.24	12.45 ± 1.51	0.5266
CVM Stage	3-4	3-4	/
BMI	18.38 ± 1.79	19.60 ± 2.55	0.1797
Transferrin (μg/μl)	5.07 ± 0.69	3.23 ± 1.71	**0.0022****
IGF-1 (ng/ml)	32.13 ± 17.88	28.98 ± 9.68	0.4713
IGFBP-3 (ng/ml)	611.78 ± 240.51	438.14 ± 154.18	0.1018

(Abbreviations: BMI, body mass index; IGF-1, insulin-like growth factor 1; IGFBP-3, insulin-like growth factor 1 binding protein-3. Data were presented as mean ± SD. **: $P<0.01$).

LysoSensor staining and V-ATPase activity assay

Cells were labeled with 2 μM LysoSensor Yellow/Blue DND-160 (Yeasen Biotechnology, 40768ES50, Shanghai, China) for 30 min at 37°C, and excessive dye was washed out using PBS. Then, the fluorescence intensity was measured using end-point mode at 37°C by a multimode microplate reader (PerkinElmer, EnSpire, Shanghai, China). Light emitted at 440 and 540 nm in response to excitation at 340 and 380 nm was measured, respectively. The ratio of fluorescence emitted at 440 and 535 nm was calculated. The V-ATPase activity of total cell lysates was assayed using V-ATPase assay kit (GENMED, GMS50247.1, Shanghai, China), and the absorbance of substrates was detected at 340 nm by a microplate reader.

Flow cytometry assay of annexin V/PI

Cells were collected using 0.25% trypsin (Gibco, 25300120, MA, U.S.A.) and washed in cooled PBS for three times. Cells were stained with annexin V and PI antibodies (Beyotime, C1062) at room temperature for 15 min, and flow cytometry analysis was performed (NovoCyte, Agilent Technology, Santa Clara, CA, U.S.A.).

Organoid culture

Mandible of C57Bl/6 mice at P4 (4 days after birth) were dissected carefully under sterile environment. After washed in PBS for three times, mandible explants were placed in organoid culture model as shown in Figure 8. Mandible organoids were cultured in DMEM with 15% fetal bovine serum and 1% penicillin-streptomycin solution. TF and 3-MA were added at concentration of 100 μg/ml and 50 μM, respectively.

Statistical analysis

All data are expressed as mean ± SD. The normality of distribution was tested by Kolmogorov–Smirnov test. If the variable was normally distributed, Student's *t*-test and one-way ANOVA would be used to analyze the between-group difference. If the variable was abnormally distributed, Mann–Whitney *U*-test or Kruskal–Wallis test would be used to perform the between-group comparison. Differences with $P<0.05$ were considered as statistically significant. Pearson correlation analysis was performed to assess the colocalization of fluorescence by ImageJ (version 1.54d, NIH, U.S.A.). All the Western blot images were quantified by ImageJ (version 1.54d). All statistical analyses were performed by using SPSS (version 19.0, IBM Corporation, New York, U.S.A.) and GraphPad Prism 5 (GraphPad Software, La Jolla, CA, U.S.A.).

Results

Serum TF level of SMH patients is significantly lower than that of normal subjects at pubertal growth peak

SMH patients were featured by small jaw, protrusive facial profile, deep overjet and mandibular deficiency (Figure 1A–C). We collected serum samples from 11 SMH patients and 14 normal subjects at pubertal growth peak (CS 3-4) (Table 3). Then, several biomarkers of bone development were detected, such as IGF-1, IGFBP-3 and TF. Interestingly, we found that serum TF level of SMH patients at growth peak was significantly lower than that of normal subjects, while other biomarkers and indexes were comparable between normal and SMH patients (Table 3 and Figure 1D). Moreover, we detected TF level in serum samples of 27 normal subjects at CS1-CS6 stage (Table 4). We found that

© 2023 The Author(s). Published by Portland Press Limited on behalf of the Biochemical Society

Table 4 Parameters of recruited normal subjects at CS1-CS6

CVM stage	Male	Female	Total	Age	Serum TF (μg/μl)	*P*-value (vs. CS6)
1	2	1	3	8.67 ± 0.58	3.37 ± 0.50	0.3051
2	2	1	3	9.67 ± 1.53	4.36 ± 0.10	**0.0113***
3	3	1	4	10.25 ± 1.26	4.74 ± 0.56	**0.0011****
4	5	5	10	11.90 ± 2.42	5.20 ± 0.72	**<0.0001*****
5	1	2	3	14.00 ± 1.00	3.29 ± 0.59	0.3713
6	2	2	4	14.3 ± 1.7	2.12 ± 1.29	/
Total	15	12	27	11.85 ± 2.77	4.17 ± 1.31	/

(Data were presented as mean ± SD, *: $P<0.05$, **: $P<0.01$, ***: $P<0.001$).

serum TF level was significantly increased as pubertal growth peak arrived (CS 3-4) and was dramatically declined after growth peak ended (CS 5-6) (Figure 1E). These results indicated that TF could play a role in mandibular growth.

TF is enriched in mandibular condylar cartilage of newborn mice and gradually declined after birth

Condylar cartilage gives rise to bone mass increment of mandible and was considered as an important growth region. Hence, in order to investigate the potential role of TF in the mandibular growth, immuno-histochemistry staining of TF was performed in condylar cartilage of C57BL/6 mice at postnatal day 0 (Day 0), day 7, week 6 and week 12, respectively. Results showed that TF was enriched in condylar cartilage of newborn mice, especially in proliferated layer and pre-hypertrophic layer, and was decreased with age (Figure 1F). Western blot analysis of condylar cartilage of C57BL/6 mice showed that the protein expression level of TF was the highest in newborn mice, and was gradually declined after birth (Figure 1G,H). These results suggested that TF could have an effect on cell survival, proliferation and chondrogenic differentiation of condylar chondrocytes.

TF not only protects chondrocytes from hypoxia-induced apoptosis but also promotes chondrocyte proliferation

Chondrogenic cell line ATDC5 cells were cultured in control medium and TF at concentration of 10 and 100 μg/ml. CCK8 assay was performed at day 0, day 1, day 2, day 3 and day 4 after cells were seeded, and result showed that TF promoted the proliferation of ATDC5 cells at dose-dependent manner (Figure 2A). In order to mimic hypoxia-induced injury, cobalt chloride ($CoCl_2$) was used to treat ATDC5 cells *in vitro*. CCK8 assay was performed at 48 h after $CoCl_2$ treatment. Results showed that the cell viability was inhibited by $CoCl_2$ and this hypoxic injury was rescued by TF administration (Figure 2B). Flow cytometry assay of Annexin V/PI showed that the population of apoptotic cells were significantly increased after $CoCl_2$ treatment, while were markedly rescued by TF at concentration of 10 and 100 μg/ml (Figure 2c,d). Moreover, Annexin V/ SYTOX staining confirmed that the number of early apoptotic cells increased significantly under hypoxic stimuli and was reduced by TF administration (Figure 2E).

TF promotes chondrogenic differentiation *in vitro*

ATDC5 cells was cultured in growth medium containing various doses of TF (0, 0.1, 1, 10, 50 and 100 μg/ml) for 9 days. Alcian blue staining showed that TF promoted chondrogenic differentiation in a dose-dependent manner (Figure 3A). RT-PCR and Western blot results confirmed that TF administration could up-regulate the mRNA and protein expression level of chondrogenic genes, including *Sox9*, *Col2a1* and *Acan* (Figure 3B–D).

TF-induced autophagy flux facilitates chondrocytes survival from hypoxia-induced apoptosis and chondrogenic differentiation

Next, we explored whether TF protected chondrocytes from hypoxia-induced apoptosis and promoted chondrogenic differentiation via activating autophagy. We found that the autophagy flux was activated under TF treatment by detecting protein level of LC3 I/II and SQSTM1 (Figure 4A). ATDC5 cells was infected with Ad-LC3-mCherry-GFP to monitor the autophagy flux. The number of autophagosomes (mCherry+, GFP+) and autolysosomes (mCherry+, GFP-) increased significantly under TF treatment (Figure 4B). ATDC5 cells were transfected with LysoTracker Red and LC3-GFP. Pearson's correlation analysis showed that TF promoted the fusion of autophagosome and lysosome (Figure 4C). Mitochondrion was one of cargoes of autolysosome. ATDC5 cells were loaded with LysoTracker Green

© 2023 The Author(s). Published by Portland Press Limited on behalf of the Biochemical Society

Clinical Science (2023) **137** 1431–1449
https://doi.org/10.1042/CS20230544

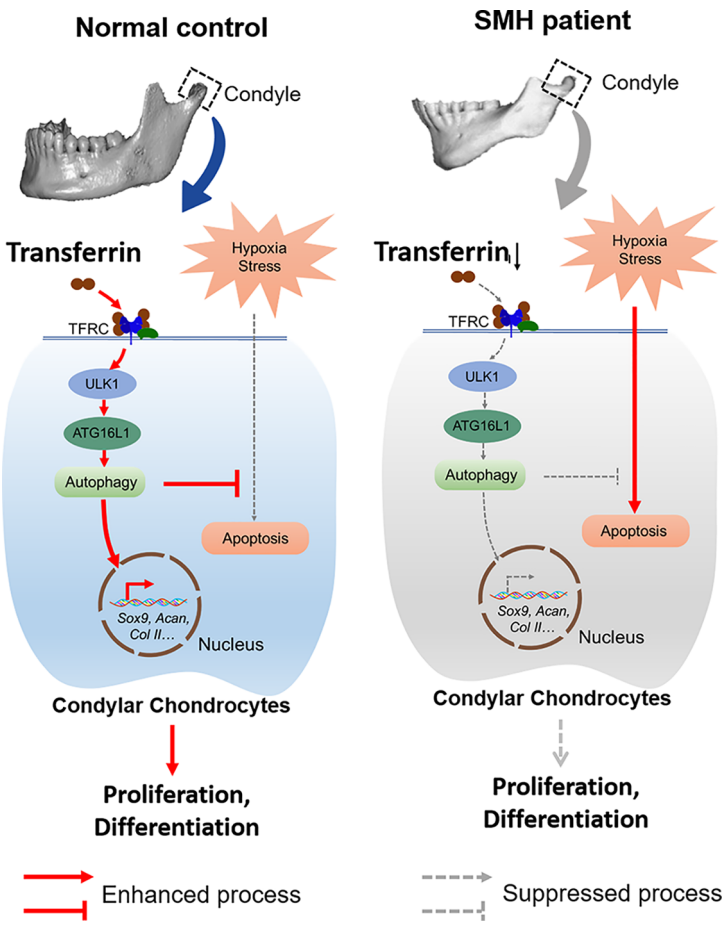

Figure 9. Graphical abstract demonstrating the mechanism of TF inducing condylar chondrocyte proliferation and chondrogenesis from hypoxia-induced apoptosis via ULK1-ATG16L1 axis

In normal subjects, TF activates autophagy via ULK1-ATG16L1 axis to protect chondrocytes from hypoxia-induced apoptosis and promote condylar chondrocyte proliferation and chondrogenesis. In SMH patients, reduced TF in condylar cartilage contributes to apoptosis of chondrocytes under hypoxia and inhibits proliferation and chondrogenesis.

and MitoTracker Red and the colocalization of the fluorescence was calculated. We found that TF promoted the engulfment of mitochondria by lysosome. (Figure 4D). Moreover, ATDC5 cells were loaded with LysoSensor DND-160 to detect the lysosomal acidity, which emitted yellow fluorescence at 540 nm in acidic lysosomes and blue fluorescence at 440 nm in less acidic or neutral lysosomes. The ratio of fluorescence intensity at 440 and 540 nm was calculated and results showed that TF promoted the acidification of lysosome (Figure 4E). The activity of V-ATPase of total cell lysates showed that TF enhanced the catalytic activity of V-ATPase (Figure 4F). In order to further assess the effect of TF on the formation of LC3 II, ATDC5 cells were incubated with 100 nM bafilomycin A1 for 4 h after cultured in TF to completely block the autophagosome–lysosome interaction. The intracellular level of LC3 II was detected by Western blot and the result showed that LC3 II accumulated more greatly in TF group than control group, indicating that TF promoted the rate of LC3 II formation (Figure 4G). ATDC5 cells transfected with Ad-mCherry-GFP-LC3 were also incubated with or without bafilomycin A1 after cultured in TF. The number of autophagosomes (yellow puncta) increased more greatly in TF group than control group after autophagosome–lysosome interaction was interrupted (Figure 4H). These results supported that TF promoted the intracellular autophagy flux.

3-MA was an autophagy inhibitor which blocked autophagic flux at initiation stage. We found that 10 μM 3-MA treatment significantly inhibited the transformation from LC3 I to LC3 II as well as the expression of COL II induced by TF (Figure 5A). Alcian blue staining showed that 3-MA could significantly block the chondrogenic promotion induced by TF (Figure 5B). Rapamycin was an autophagy activator through inhibiting mTOR complex. We found that 1 μM rapamycin treatment could significantly up-regulated the expression of COL II induced by TF (Figure 5C). Alcian blue staining also showed that rapamycin could significantly promoted the chondrogenic effect of TF

© 2023 The Author(s). Published by Portland Press Limited on behalf of the Biochemical Society

(Figure 5D). Flow cytometry of annexin V/ PI staining showed that 3-MA treatment partially blocked the effect of TF on protection from hypoxia-induced apoptosis (Figure 5E). These results suggested that TF-induced autophagy facilitated the chondrogenic differentiation and cell survival from hypoxia.

TF induces autophagy flux via ULK1-ATG16L1 axis

To explore the mechanism underlying the activation of autophagy flux induced by TF, we analyzed the mRNA level of main autophagy-related genes (ATGs) after TF treatment by RT-PCR. The mRNA level of *Atg16l1* was found to elevate significantly under TF treatment (Figure 6A). Western blot detected that protein level of ATG16L1 increased significantly under TF treatment (Figure 6B). Immunofluorescence staining of ATG16L1 revealed that the number of ATG16L1+ puncta per cell increased significantly under TF treatment. Rapamycin was used as a positive control (Figure 6C,D).

ATG16L1 was reported to be one of downstream targets of ULK1, a key kinase that triggered the initiation of autophagy via phosphorylation on Ser555 by AMPK. We detected that the level of TF receptor (TFRC), phospho-AMPKα and phospho-ULK1^{Ser555} were significantly increased under TF treatment (Figure 7A). Knockdown of *Tfr1*, *Ulk1/2* or *Atg1611* by siRNA could block the autophagy activation induced by TF treatment (Figure 7B). Ad-LC3-mCherry-GFP infection confirmed that the silence of ULK1-ATG16L1 axis significantly inhibited the formation of autophagosomes and autolysosomes induced by TF (Figure 7C,D). Meanwhile, Alcian blue staining showed that the chondrogenesis induced by TF was inhibited after ULK1-ATG16L1 axis was silenced (Figure 7E). Fluorescence staining of annexin V/ SYTOX showed that the anti-apoptosis function of TF was partially blocked by knocking down *Tfr1*, *Ulk1/2* or *Atg16l1* (Figure 7F). These results suggested that TF stimulated autophagy flux through ULK1-ATG16L1 axis, facilitating chondrocytes survival from hypoxia-induced apoptosis and chondrogenic differentiation *in vitro*.

TF promotes condylar growth and chondrogenesis of mandible organoid

We established an *ex vivo* culture model of mandible based on the protocol proposed by Wiszniak et al [22] (Figure 8A,B). Mandible explants was cultured in control medium (Blank), TF medium (TF) and TF medium with 3-MA (TF+3-MA), respectively. After cultured for 7 days, the cartilaginous layer of mandible cultured in TF medium was significantly thicker compared with control group, while mandible cultured in TF+3-MA medium showed no significant change (Figure 8C). Micro-CT analysis was performed to assess the subchondral bone of condyle. Results showed that the BV/TV, the thickness of trabecular bone, the length of condylar neck and mandible in TF group were significantly higher than control group. This promotion effect was partially blocked by autophagy inhibitor 3-MA (Figure 8D,E), confirming that TF promotes condylar growth and chondrogenesis partly via up-regulating autophagy. Toluidine blue staining (Figure 8F) and immunostaining of COL II and ACAN (Figure 8G) were performed on slices of condylar cartilage. Results showed that TF promoted chondrogenic differentiation of condylar chondrocytes, and blocking autophagy could partially reverse the promotion effect of TF. Our results indicated that TF protected chondrocytes from hypoxia-induced apoptosis and promoted chondrocytes differentiation through inducing autophagy via ULK1-ATG16L1 axis, therefore promoted condylar growth and mandibular bone mass increment (Figure 9).

Discussion

Skeletal mandibular hypoplasia was often accompanied by increasing apoptosis and impaired chondrogenesis of condylar chondrocytes [9,10]. Our study unraveled that transferrin (TF), which was enriched in condylar cartilage, exhibited protective effect on chondrocytes from apoptosis and promoted proliferation and differentiation of chondrocytes via activating autophagy, thereby advancing our knowledge of the mechanism underlying the development of condylar cartilage and shedding new light on developing treatment strategy of SMH patients.

The first new finding of our study is that we unravel a novel role of TF in enhancing proliferation and differentiation of chondrocytes. Although TF has been widely believed to be important for iron transport and iron acquisition by mammalian cells [23], its physiological function in proliferation and differentiation was seldom reported. Pérez et al. revealed that TF enhanced neuronal differentiation *in vitro*, indicating that TF could be a promising candidate to be used in regenerative strategies for neurodegenerative diseases [24]. However, to the best of our knowledge, the role of TF in chondrogenesis and osteogenesis in bone development is poorly understood. Malecki et al. reported that mice with hypotransferrinemia (less than 1% of normal plasma TF concentrations) showed dwarfism and abnormal bone mechanical properties of tibia, but the underlying mechanism still remained unclear [25]. Our study proved that TF enhanced differentiation and proliferation of chondrocytes *in vitro*, and promoted condylar growth at organoid level, suggesting a novel role of TF in enhancing proliferation and differentiation of chondrocytes.

© 2023 The Author(s). Published by Portland Press Limited on behalf of the Biochemical Society

Clinical Science (2023) **137** 1431–1449
https://doi.org/10.1042/CS20230544

The second new finding of the manuscript is that we reveal a new mechanism by which TF promotes chondrocyte proliferation via autophagy through ULK1-ATG16L1 axis. Although TFRC is reported to contribute to autophagosome formation [26], the mechanism of TF inducing autophagy flux is largely unknown. In the present study, we find that TF promotes chondrocyte proliferation via autophagy flux via ULK1-ATG16L1 axis. ATG16L1 is reported to play a role in autophagosome initiation, membrane nucleation and membrane expansion in autophagy flux. At initiation stage, ULK1 activates PI3K complex via BECN1 to produce PtdIns3P in membranes related to autophagosome biogenesis, thereby recruiting WIPI2 and ATG16L1 on RAB11A positive compartments to form ATG16L1 dimers [27,28]. Then, the ATG16L1 dimers interacted with ATG12-ATG5 conjugates to form the ATG12-ATG5-ATG16L1 complex and exerted E3 enzyme activity that promotes the lipid conjugation reaction of LC3 [29]. Alsaadi et al. find that ATG16L1 is a novel target of ULK1. ULK1 kinase directly phosphorylates ATG16L1 to enhance its function in response to starvation and infection [30]. Our research detected that TF treatment could activate ULK1^{Ser555} to improve the expression level of ATG16L1 and promote autophagy flux, thereby confirming the enhancement effect of ULK1-ATG16L1 axis on autophagy flux.

Apart from the detected ULK1-ATG16L1 signaling, TF treatment may promote the expression of ATG16L1 in other pathways. ATG16L1 is located on cell membrane and is one of multiple membrane sources of autophagosome [31]. ATG16L1 associated with clathrin-coated pits, and after internalization and uncoating, the ATG16L1-associated plasma membrane became associated with phagophore precursors, which matured into phagophores and then autophagosomes [31,32]. Our study detected that TF significantly increased the number of ATG16L1+ puncta. Ivanova et al. find that rapid uptake via clathrin-mediated endocytosis can activate autophagy [33]. Considering that TF enters cells via clathrin-mediated endocytosis, the entry of TF can promote the formation of ATG16L1+ vesicles via an unknown mechanism that involved in clathrin recruitment, uncoating or vesicle cleavage, which needs further investigation [34,35].

The third new finding of the research is that we prove that TF is highly expressed in avascular condylar cartilage and can promote condylar growth at organoid level. Previous studies believed that TF was mainly enriched in tissues containing abundant bloodstream and in great need for serum iron, such as liver, bone marrow and skeletal muscle [23]. But whether TF was expressed in cartilage was still not clear. Our study found that TF was enriched in condylar cartilage, especially in proliferative and pre-hypertrophic layer. Previous studies reported that the uptake and intracellular transport of TF was regulated by the oxygen and nutrition level of microenvironment. Under hypoxic or starved condition, the uptake of TF was significantly enhanced [36,37]. Since cartilage was reported to be an avascular tissue lack of oxygen and nutrients [38], this might be a reasonable explanation for the abundant intracellular storage of TF in proliferative and pre-hypertrophic chondrocytes. Moreover, we proved that TF promoted condylar growth at organoid level, which shed new light on developing treatment strategy of SMH patients.

Another factor that may have influence on the chondrogenic effect and autophagic flux induced by TF was iron ion. We detected the level of serum iron and ferritin of control and SMH patients and no significant difference was found (Supplementary Figure S1), indicating that there was at least no defect on iron storage in SMH patients. Besides, we also detected the intracellular iron level after TF treatment, and found that the intracellular iron level was significantly reduced in TF group than control group (data not shown), probably due to the chelation effect of apo-transferrin on iron ion [39]. Previous studies reported that iron overload could impair intracellular autophagy [40], while iron efflux could activate autophagic flux through stabilization of HIF-1a [41]. Therefore, the iron efflux may partly contribute to the autophagic flux induced by TF, and further studies were needed to elucidate the molecular mechanism.

Collectively, our study unraveled a novel role of TF in protection from hypoxia-induced apoptosis and promoting proliferation and differentiation of chondrocytes through inducing autophagy flux via ULK1-ATG16L1 axis. Even though the organoid culture has confirmed the enhancement effect of TF on growth of condylar cartilage, further studies are still needed to verify this effect *in vivo*, as well as to create a safe and highly-efficient delivery vehicle targeting condylar chondrocytes to promote condylar growth of SMH patients.

Clinical perspectives

- Skeletal mandibular hypoplasia (SMH) is one of the most common skeletal craniofacial deformities in orthodontics. Detecting the pathogenesis of SMH and developing efficient therapy strategies to promote mandibular growth are vital for treatment of SMH. In the present study, we found a significant difference in serum level of TF between normal subjects and SMH patients. However, the function and underlying mechanism of TF in condylar growth still remained unclear.

© 2023 The Author(s). Published by Portland Press Limited on behalf of the Biochemical Society

- TF was highly expressed in condylar cartilage of newborn mice and was gradually decreased as condylar cartilage ceased growing. TF protected chondrocytes from hypoxia-induced apoptosis and promoted proliferation and differentiation of chondrocytes through activating autophagy via ULK1-ATG16L1 axis. Moreover, TF promoted condylar growth and endochondral ossification at organoid level.
- We demonstrated that TF played a key role in condylar growth. Thus, TF could be a potential novel growth factor of condylar cartilage, which shed new light on developing treatment strategy of SMH patients.

Data Availability

The data underlying this article will be shared on reasonable request to the corresponding author.

Competing Interests

The authors declare that there are no competing interests associated with the manuscript.

Funding

This work was supported by National Natural Science Foundation of China [grant numbers 81970979 and 81771027] and China Postdoctoral Science Foundation [grant number 2022M710255].

Author Contribution

Xi Wen: Conceptualization, Data curation, Software, Formal analysis, Investigation, Methodology, Writing—original draft, Funding acquisition. **Yixiang Wang:** Supervision, Methodology, Writing—review & editing. **Yan Gu:** Conceptualization, Resources, Supervision, Funding acquisition, Validation, Writing—review & editing.

Ethics Statement

The research protocol was approved by Biomedical Ethics Committee of Peking University School and Hospital of Stomatology (PKUSSIRB-201735069, 202055072). Informed consents were obtained from both patients and their parents. The study was performed in accordance with the World Medical Association Declaration of Helsinki.

Abbreviations

ATG, autophagy-related gene; ELISA, enzyme-linked immunosorbent assay; PVDF, polyvinylidene difluoride; SMH, skeletal mandibular hypoplasia; TF, transferrin; TFRC, transferrin receptor.

References

1 Zhao, J., Zhou, X., Tang, Q., Yu, R., Yu, S., Long, Y. et al. (2018) BMAL1 deficiency contributes to mandibular dysplasia by upregulating MMP3. *Stem Cell Rep.* **10**, 180–195, https://doi.org/10.1016/j.stemcr.2017.11.017
2 Bibbins-Domingo, K., Grossman, D.C., Curry, S.J., Davidson, K.W., Epling, J.J., Garcia, F.A. et al. (2017) Screening for obstructive sleep apnea in adults: US Preventive Services Task Force Recommendation Statement. *JAMA* **317**, 407–414, https://doi.org/10.1001/jama.2016.20325
3 Cozza, P., Baccetti, T., Franchi, L., De Toffol, L. and McNamara, J.J. (2006) Mandibular changes produced by functional appliances in Class II malocclusion: a systematic review. *Am. J. Orthod. Dentofacial Orthop.* **129**, 591–599, e1-e6, https://doi.org/10.1016/j.ajodo.2005.11.010
4 Bidjan, D., Sallmann, R., Eliades, T. and Papageorgiou, S.N. (2020) Orthopedic treatment for class II malocclusion with functional appliances and its effect on upper airways: a systematic review with meta-analysis. *J. Clin. Med.* **9**, 3806–3823, https://doi.org/10.3390/jcm9123806
5 Zhou, X., Yu, R., Long, Y., Zhao, J., Yu, S., Tang, Q. et al. (2018) BMAL1 deficiency promotes skeletal mandibular hypoplasia via OPG downregulation. *Cell Proliferat* **51**, e12470, https://doi.org/10.1111/cpr.12470
6 Berraquero, R., Palacios, J. and Rodriguez, J.I. (1992) The role of the condylar cartilage in mandibular growth. A study in thanatophoric dysplasia. *Am. J. Orthod. Dentofacial Orthop.* **102**, 220–226, https://doi.org/10.1016/S0889-5406(05)81056-X
7 Copray, J.C., Dibbets, J.M. and Kantomaa, T. (1988) The role of condylar cartilage in the development of the temporomandibular joint. *Angle Orthod.* **58**, 369–380
8 Kozhemyakina, E., Lassar, A.B. and Zelzer, E. (2015) A pathway to bone: signaling molecules and transcription factors involved in chondrocyte development and maturation. *Development* **142**, 817–831, https://doi.org/10.1242/dev.105536
9 Tang, Y., Hong, C., Cai, Y., Zhu, J., Hu, X., Tian, Y. et al. (2020) HIF-1α mediates osteoclast-induced mandibular condyle growth via AMPK signaling. *J. Dent. Res.* **99**, 1377–1386, https://doi.org/10.1177/0022034520935788

© 2023 The Author(s). Published by Portland Press Limited on behalf of the Biochemical Society

10 Yu, S., Tang, Q., Xie, M., Zhou, X., Long, Y., Xie, Y. et al. (2020) Circadian BMAL1 regulates mandibular condyle development by hedgehog pathway. *Cell Proliferat* **53**, e12727–e12737, https://doi.org/10.1111/cpr.12727
11 van Gastel, N., Stegen, S., Eelen, G., Schoors, S., Carlier, A., Daniëls, V.W. et al. (2020) Lipid availability determines fate of skeletal progenitor cells via SOX9. *Nature* **579**, 111–117, https://doi.org/10.1038/s41586-020-2050-1
12 Yao, Q., Khan, M.P., Merceron, C., LaGory, E.L., Tata, Z., Mangiavini, L. et al. (2019) Suppressing mitochondrial respiration is critical for hypoxia tolerance in the fetal growth plate. *Dev. Cell.* **49**, 748–763, https://doi.org/10.1016/j.devcel.2019.04.029
13 van Gastel, N. and Carmeliet, G. (2021) Metabolic regulation of skeletal cell fate and function in physiology and disease. *Nat. Metab.* **3**, 11–20, https://doi.org/10.1038/s42255-020-00321-3
14 Horigome, Y., Ida-Yonemochi, H., Waguri, S., Shibata, S., Endo, N. and Komatsu, M. (2020) Loss of autophagy in chondrocytes causes severe growth retardation. *Autophagy* **16**, 501–511, https://doi.org/10.1080/15548627.2019.1628541
15 Hu, S., Zhang, C., Ni, L., Huang, C., Chen, D., Shi, K. et al. (2020) Stabilization of HIF-1α alleviates osteoarthritis via enhancing mitophagy. *Cell Death Dis.* **11**, 481–496, https://doi.org/10.1038/s41419-020-2680-0
16 Liu, W., Luo, H., Wang, R., Kang, Y., Liao, W., Sun, Y. et al. (2020) Rapamycin-induced autophagy promotes the chondrogenic differentiation of synovium-derived mesenchymal stem cells in the temporomandibular joint in response to IL-1β. *Biomed. Res. Int.* **2020**, 1–12, https://doi.org/10.1155/2020/4035306
17 Kang, X., Yang, W., Feng, D., Jin, X., Ma, Z., Qian, Z. et al. (2017) Cartilage-specific autophagy deficiency promotes ER stress and impairs chondrogenesis in PERK-ATF4-CHOP-dependent manner. *J. Bone Miner. Res.* **32**, 2128–2141, https://doi.org/10.1002/jbmr.3134
18 Gomme, P.T., McCann, K.B. and Bertolini, J. (2005) Transferrin: structure, function and potential therapeutic actions. *Drug Discov. Today* **10**, 267–273, https://doi.org/10.1016/S1359-6446(04)03333-1
19 Lei, R., Zhang, K., Liu, K., Shao, X., Ding, Z., Wang, F. et al. (2016) Transferrin receptor facilitates TGF-β and BMP signaling activation to control craniofacial morphogenesis. *Cell Death Dis.* **7**, e2282, https://doi.org/10.1038/cddis.2016.170
20 Baccetti, T., Franchi, L. and McNamara, J. (2005) The cervical vertebral maturation (CVM) method for the assessment of optimal treatment timing in dentofacial orthopedics. *Semin. Orthod.* **11**, 119–129, https://doi.org/10.1053/j.sodo.2005.04.005
21 Chow, S., Shao, J. and Wang, H. (2008) *Sample Size Calculations in Clinical Research*, 2nd Ed, Chapman & Hall/CRC Press, Boca Raton
22 Wiszniak, S. and Schwarz, Q. (2022) Mandible explant assay for the analysis of Meckel's cartilage development. *Methods Mol. Biol.* **2403**, 235–247, https://doi.org/10.1007/978-1-0716-1847-9˙16
23 Kawabata, H. (2019) Transferrin and transferrin receptors update. *Free Radical Bio. Med.* **133**, 46–54, https://doi.org/10.1016/j.freeradbiomed.2018.06.037
24 Pérez, M.J., Carden, T.R., Dos Santos Claro, P.A., Silberstein, S., Páez, P.M., Cheli, V.T. et al. (2023) Transferrin enhances neuronal differentiation. *Asn Neuro* **15**, 166769435, https://doi.org/10.1177/17590914231170703
25 Malecki, E.A., Buhl, K.M., Beard, J.L., Jacobs, C.R., Connor, J.R. and Donahue, H.J. (2000) Bone structural and mechanical properties are affected by hypotransferrinemia but not by iron deficiency in mice. *J. Bone Miner. Res.* **15**, 271–277, https://doi.org/10.1359/jbmr.2000.15.2.271
26 Longatti, A. and Tooze, S.A. (2012) Recycling endosomes contribute to autophagosome formation. *Autophagy* **8**, 1682–1683, https://doi.org/10.4161/auto.21486
27 Puri, C., Vicinanza, M., Ashkenazi, A., Gratian, M.J., Zhang, Q., Bento, C.F. et al. (2018) The RAB11A-positive compartment is a primary platform for autophagosome assembly mediated by WIPI2 recognition of PI3P-RAB11A. *Dev. Cell.* **45**, 114–131, https://doi.org/10.1016/j.devcel.2018.03.008
28 Salem, M., Ammitzboell, M., Nys, K., Seidelin, J.B. and Nielsen, O.H. (2015) ATG16L1: A multifunctional susceptibility factor in Crohn disease. *Autophagy* **11**, 585–594, https://doi.org/10.1080/15548627.2015.1017187
29 Nakatogawa, H. (2020) Mechanisms governing autophagosome biogenesis. *Nat. Rev. Mol. Cell Biol.* **21**, 439–458
30 Alsaadi, R.M., Losier, T.T., Tian, W., Jackson, A., Guo, Z., Rubinsztein, D.C. et al. (2019) ULK1-mediated phosphorylation of ATG16L1 promotes xenophagy, but destabilizes the ATG16L1 Crohn's mutant. *EMBO Rep.* **20**, e46885–e46896, https://doi.org/10.15252/embr.201846885
31 Puri, C., Renna, M., Bento, C.F., Moreau, K. and Rubinsztein, D.C. (2013) Diverse autophagosome membrane sources coalesce in recycling endosomes. *Cell* **154**, 1285–1299, https://doi.org/10.1016/j.cell.2013.08.044
32 Moreau, K., Ravikumar, B., Renna, M., Puri, C. and Rubinsztein, D.C. (2011) Autophagosome precursor maturation requires homotypic fusion. *Cell* **146**, 303–317, https://doi.org/10.1016/j.cell.2011.06.023
33 Ivanova, M.M., Dao, J., Kasaci, N., Adewale, B., Fikry, J. and Goker-Alpan, O. (2020) Rapid clathrin-mediated uptake of recombinant α-Gal-A to lysosome activates autophagy. *Biomolecules* **10**, 837, https://doi.org/10.3390/biom10060837
34 Miller, K., Shipman, M., Trowbridge, I.S. and Hopkins, C.R. (1991) Transferrin receptors promote the formation of clathrin lattices. *Cell* **65**, 621–632, https://doi.org/10.1016/0092-8674(91)90094-F
35 Liu, A.P., Aguet, F., Danuser, G. and Schmid, S.L. (2010) Local clustering of transferrin receptors promotes clathrin-coated pit initiation. *J. Cell Biol.* **191**, 1381–1393, https://doi.org/10.1083/jcb.201008117
36 Dauner, K., Eid, W., Raghupathy, R., Presley, J.F. and Zha, X. (2017) mTOR complex 1 activity is required to maintain the canonical endocytic recycling pathway against lysosomal delivery. *J. Biol. Chem.* **292**, 5737–5747, https://doi.org/10.1074/jbc.M116.771451
37 Lok, C.N. and Ponka, P. (1999) Identification of a hypoxia response element in the transferrin receptor gene. *J. Biol. Chem.* **274**, 24147–24152, https://doi.org/10.1074/jbc.274.34.24147
38 Hollander, J.M. and Zeng, L. (2019) The emerging role of glucose metabolism in cartilage development. *Curr. Osteoporos Rep.* **17**, 59–69, https://doi.org/10.1007/s11914-019-00506-0
39 Chen-Roetling, J., Chen, L. and Regan, R.F. (2011) Apotransferrin protects cortical neurons from hemoglobin toxicity. *Neuropharmacology* **60**, 423–431, https://doi.org/10.1016/j.neuropharm.2010.10.015

© 2023 The Author(s). Published by Portland Press Limited on behalf of the Biochemical Society

40 Uberti, V.H., de Freitas, B.S., Molz, P., Bromberg, E. and Schröder, N. (2020) Iron overload impairs autophagy: effects of rapamycin in ameliorating iron-related memory deficits. *Mol. Neurobiol.* **57**, 1044–1054, https://doi.org/10.1007/s12035-019-01794-4

41 Wu, Y., Li, X., Xie, W., Jankovic, J., Le, W. and Pan, T. (2010) Neuroprotection of deferoxamine on rotenone-induced injury via accumulation of HIF-1α and induction of autophagy in SH-SY5Y cells. *Neurochem. Int.* **57**, 198–205, https://doi.org/10.1016/j.neuint.2010.05.008

© 2023 The Author(s). Published by Portland Press Limited on behalf of the Biochemical Society